Journal of CO2 Utilization 85 (2024) 102865

Contents lists available at ScienceDirect

Journal of CO2 Utilization

journal homepage: www.elsevier.com/locate/jcou

Halloysite-kojic acid conjugate: A sustainable material for the photocatalytic CO_2 reduction and fixation for cyclic carbonates production

Erika Saccullo [a,b], Vincenzo Patamia [a,*], Federica Magaletti [c], Giusy Dativo [d], Monia Camarda [a], Roberto Fiorenza [d], Vincenzina Barbera [c], Giuseppe Floresta [a,*], Antonio Rescifina [a]

[a] Department of Drug and Health Sciences, University of Catania, Viale Andrea Doria 6, Catania 95125, Italy
[b] Department of Biomedical and Biotechnological Sciences (Biometec), University of Catania, Via Santa Sofia 97, Catania 95123, Italy
[c] Department of Chemistry, Materials and Chemical Engineering (Giulio Natta), Politecnico di Milano, Via Mancinelli 7, Milano, Italy
[d] Department of Chemical Sciences, University of Catania, Viale Andrea Doria 6, Catania 95125, Italy

ARTICLE INFO

Keywords:
CO_2
Kojic acid
Halloysite
Cyclic carbonates
Sustainable material

ABSTRACT

This study introduces a straightforward synthesis method for producing a hybrid material composed of halloysite and kojic acid, which catalyzes carbon dioxide (CO_2) conversion processes. Kojic acid, derived from malted rice fermentation, exhibits inherent chelating properties that facilitate the introduction of copper ions onto the material's surface. Copper ions, an economically viable alternative to noble metals, catalyze CO_2 conversion reactions effectively. The hybrid catalyst was evaluated for two distinct CO_2 conversion pathways: photocatalytic methane production under simulated sunlight and CO_2 fixation into cyclic carbonates via epoxide reactions. The hybrid material demonstrates remarkable catalytic activity under mild conditions, achieving high conversion efficiencies at 45 °C for methane production and 70 °C for carbonate fixation at atmospheric pressure. Conversion of 31 % and 89 % were achieved for the photocatalytic CO_2 reduction and the carbonate fixation, respectively. FT-IR spectra confirmed the functionalization of the material. Additionally, its organic/inorganic hybrid nature is complemented by excellent thermal stability, as studied by TGA. It enables repeated utilization, maintaining a 25 % catalytic activity for methane production and 70 % for carbonate fixation after the fourth reuse. This research highlights the potential of using naturally derived materials for sustainable CO_2 mitigation.

1. Introduction

Halloysite clay nanotubes (HNTs) have emerged as versatile and sustainable nanocomposites with several applications spanning from catalysis to drug delivery and environmental applications. One prominent area where HNTs have demonstrated promising performance is heterogeneous catalysis, where its tubular morphology lends itself well to catalyst separation and recyclability, as well as its high porosity that was largely exploited as catalytic support [1,2]. Numerous halloysite-based heterogeneous catalysts have been developed recently, demonstrating excellent catalytic performance and synergism between halloysite and other composite/hybrid components [3–5]. Moreover, HNTs have been recognized by several researchers for their value in CO_2 valorization [6–9]. In particular, their green nature and basic sites can be exploited in interesting environmental applications, such as the conversion of carbon dioxide into methane and other valuable products through organic synthesis [10], or CO_2 capture [11]. In this context, exploring halloysite's potential as a catalyst for CO_2 conversion and its applications in ^{11}C labeling demonstrate the versatile nature of this mineral and its contribution to addressing environmental challenges and advancing scientific knowledge. Furthermore, in recent years, halloysite-based materials have also been used in the field of photochemistry, and photocatalysis has seen an increasing focus on using metal-organic hybrid materials for the photoconversion of CO_2 [12–15]. These materials, composed of metals and organic molecules, can absorb sunlight to trigger chemical reactions that convert CO_2 into high-added value products such as methane. The conversion of CO_2 into methane represents a promising solution for reducing the environmental impact caused by the increasing concentration of CO_2 in the atmosphere. The methane produced can be used as a renewable energy source and thus contribute to the reduction of greenhouse gas emissions. However, for this technology to be effectively implemented on an industrial scale, new materials capable of carrying out this reaction efficiently and selectively must be developed. Therefore, synthesizing metal-organic

* Corresponding authors.
E-mail addresses: vincenzo.patamia@unict.it (V. Patamia), giuseppe.floresta@unict.it (G. Floresta).

https://doi.org/10.1016/j.jcou.2024.102865
Received 3 June 2024; Received in revised form 29 June 2024; Accepted 3 July 2024
Available online 15 July 2024

hybrid materials with optimal properties for the photoconversion of CO_2 is a crucial step toward realizing a sustainable and environmentally friendly conversion system [16–20]. Likewise, the importance of converting CO_2 and fixing it in reusable organic compounds lies in the need to reduce the impact of greenhouse gases on the environment and to valorize CO_2 as a resource instead of waste.

In this paper, we report the simple synthesis of a hybrid inorganic-organic material based on HNT and kojic acid (K), which serves as a catalyst for the valorization of CO_2 through two distinct reactions and catalytic approaches. K, a natural by-product of the fermentation process of malted rice [21], is known for its ability to chelate various metal ions. For instance, it forms a bright red complex with ferric ions [22,23], a property utilized in the food and cosmetics industry for preservation and color modification [24]. Leveraging the chelating capabilities of K, we introduced copper ions, which are economical and non-critical compared to widely used noble metals, as active species for the CO_2 conversion reactions [25–27] to investigate the photoconversion of CO_2 into methane through simulated sunlight, and the fixation of CO_2 into cyclic carbonates, in the absence of copper, by reaction with epoxides. The hybrid material demonstrated excellent catalytic performance in both applications, achieving high conversion and fixation rates under relatively mild reaction conditions. The yields obtained were impressive, highlighting the potential of HNT-K hybrid materials as effective catalysts in CO_2 valorization processes.

2. Materials and methods

2.1. General Information

All the required chemicals were purchased from Merck and VWR. Precoated aluminum sheets (silica gel 60 F254, Merck) were used for thin-layer chromatography (TLC) and visualized under UV light. ^{1}H NMR spectra were recorded at 300 K on Varian UNITY Inova using $CDCl_3$ as the solvent at 500 MHz for ^{1}H NMR. Chemical shift (δ) values were given in ppm.

2.2. Synthesis of materials

2.2.1. General procedure for the synthesis of HNT-K catalyst

The procedure was modified from that reported in a previous work [28]. HNT (400 mg) was added to a 10 mL round-bottomed reaction flask containing DMF (2 mL); the amount in moles of Et_3N was related to the amount of ClK acid to obtain HNT-K1, HNT-K3, and HNT-K6 (Table 1) and the mixture was magnetically stirred at room temperature for 30 min. Next, the appropriate amount by weight of ClK was added to obtain HNT-K1, HNT-K3, and HNT-K6 (Table 1), and the reaction mixture was left to stir overnight at 80 °C. Then, the precipitate was collected by filtration, washed several times with acetone (5 × 10 mL), and placed in an oven at 65 °C overnight.

2.2.2. General procedure for the synthesis of HNT-K6D

HNT-K6 (100 mg) was added to a 10 mL round-bottomed reaction flask containing 5 mL of 1 M KOH in water. The suspension was stirred for 2 h and then filtered and dried. 5 mL of 1 M solution of DCl in D_2O was then added to the dried powder and stirred for 2 h. HNT-K6D was then recovered as filtrate and dried.

Table 1
Screening of different weight (wt) ratios between HNT and K.

Entry	HNT:K (wt/wt) [a]	Et_3N (eq.)	Sample
1	1:1	2	HNT-K1
2	1:3	6	HNT-K3
3	1:6	10	HNT-K6

[a] All reactions were performed in DMF at 80 °C overnight.

2.2.3. General procedure for the synthesis of HNT-K/Cu

The complexation and reduction reactions were performed by varying the procedure reported in the literature [29]. HNT-K1, HNT-K3, and HNT-K6 (100 mg) were dispersed in 2, 4, and 8 mL of H_2O to which 0.125, 0.376, and 0.751 g of $CuCl_2$ (powder, 99 % by Sigma-Aldrich, product number: 751944–25 G) maintained under stirred at 55 °C overnight, respectively, was added. After completion, the solvents were removed under reduced pressure to get a pure product. The product was subsequently washed several times with deionized H_2O and centrifuged to remove excess uncomplexed Cu.

For the reduction from Cu(II) to Cu(I) to the obtained products HNT-K1/Cu(II), HNT-K3/Cu(II), and HNT-K6/Cu(II), 2, 4, and 6 mL of an ascorbic acid solution 0.5 M were added to the slurry. The dispersion was left to stir for 3 h at r.t. Finally, the slurry obtained was centrifuged at 950 rpm for 10 min 3 times and washed several times with deionized water and acetone. The supernatant was removed, and the slurry was dried under vacuum.

2.3. Experimental setup

2.3.1. General procedure for the solar photocatalytic CO_2 reduction

The photocatalytic measurements were carried out at atmospheric pressure with a cylindrical batch Pyrex reactor, filled with 0.1 g of sample, irradiating for 7 h with a solar lamp (Osram Ultra Vitalux 300 W, irradiance of 10.7 mW/cm^2). A mixture of CO_2 (99.999 %) and H_2 gas (produced by an HK Hydrogen generator, purity 99.9996 %) was flowed in the photoreactor to permit the saturation of the sample surface with the reagent molecules. With a mass flow controller, the H_2/CO_2 mixture was tuned to favor the CO_2 methanation (H_2:CO_2 molar ratio 4:1) [30].

The reaction products (in our experimental conditions, only CO and CH_4) were examined with the Agilent 6890 N gas chromatograph (HP-PLOT Q column, TCD detector) and with the Trace GC instrument (Porapak Q column, FID detector) adequately calibrated. The measurements were replied to three times (3 % experimental error).

The CO_2 conversion values were calculated with the Eq. 1:

$$CO_2\text{conversion\%}: \left(\frac{\text{Area}_{\text{peak CO2in}} - \text{Area}_{\text{peak CO2out}} \times \left(\frac{\text{Area}_{\text{peak standard in}}}{\text{Area}_{\text{peak standard out}}} \right)}{\text{Area}_{\text{peakCO2in}}} \right) \times 100 \quad (1)$$

Moreover, also the mass balance method was applied, considering the Eq. 2:

$$CO_2\text{conversion\%}: \left(\frac{\text{Area}_{\text{peak CO2out}}}{\text{Area}_{\text{peak products out}} + \text{Area}_{\text{peak CO2out}}} \right) \times 100 \quad (2)$$

The two methods were in accordance with each other (± 5 %, reproducibility 95 %).

The selectivity to CO and CH_4 products on an electron basis was evaluated with Eqs. 3 and 4 [31]:

$$CH_4\text{selectivity\%}: \left(\frac{8N_{CH4}}{(8N_{CH4} + 2N_{CO})} \right) \times 100 \quad (3)$$

$$\text{CO selectivity\%}: \left(\frac{2N_{CO}}{(8N_{CH4} + 2N_{CO})} \right) \times 100 \quad (4)$$

where N_{CH4} and N_{CO} are the production rates of CH_4 and CO in μmol/$g_{catalyst}$•$h_{irradiation}$ and the coefficients 8 and 2, are used to account the electrons involved in the photocatalytic reduction reactions to form CH_4 and CO from the CO_2 using H_2 as the electron donor and proton resource, considering the reactions (a) and (b) [32–34]:

(a) $CO_2 + 2\,H^+ + 2e^- \rightarrow CO + H_2O$

(b) $CO_2 + 8\ H^+ + 8e^- \rightarrow CH_4 + 2\ H_2O$

The CH_4 yield (%) was calculated with the following Eq. 5:

$$CH_4 yield\% : \left(\frac{(CH_4 selectvity\% \times CO_2 conversion\%}{100}\right) \quad (5)$$

2.3.2. General procedure for the CO_2 adsorption test

The CO_2 adsorption tests were conducted in a homemade quartz reactor filled with 100 mg of the analyzed powder. A 30 mL/min flow of CO_2 (99.999 %) was sent inside the reactor at atmospheric pressure and room temperature. The CO_2 was detected by an online quadrupole mass spectrometer (Sensorlab VG Quadrupoles) following the $m/z = 44$ signal. The CO_2 breakthrough curves were evaluated by measuring the ratio between the concentration of CO_2 after the achievement of saturation in the sample and the CO_2 concentration (i.e., without the sample) [35]. Before the determination, the samples were pretreated in He flows (30 mL/min) for 2 h to remove eventual contaminants from the sample surface.

2.3.3. General procedure for the synthesis of cyclic carbonate

The catalytic reaction of CO_2 was carried out without solvent. Epoxide (10 mmol), HNT-K6 catalyst (5 %wt), and TBAB as a co-catalyst (0.5 mmol) were added at the same time in a vial, and the reaction was stirred under CO_2 flux (1 atm) at 70 °C per 10 h. At the end of the reaction, the products were extracted with chloroform to separate them from the catalyst and purified by flash chromatographic column cyclohexane: ethyl acetate 8:2 as eluent. The products were characterized by ^{1}H NMR; see Supporting Information (Figs. S1–S4).

HNT-K6, which is not soluble in the organic solvent, was vacuum-dried after separation by centrifugation for reuse in subsequent processes. This procedure was repeated three times to ensure no residual products remained on the catalyst.

The reaction time of frequency (TOF) was calculated considering the yield obtained in the presence of both HNT-K6 and TBAB (P_{AB}), the yield obtained only in the presence of TBAB (P_B), the reaction time in hours (t), and the mol% of HNT-K6 (A_0) (Eq. 6). mol% was calculated considering only the amount of K calculated through Eq. 7 [36]:

$$TOF \approx \frac{(P_{AB} - P_B)}{t \bullet A_0} \quad (6)$$

2.4. Characterization

2.4.1. Infrared spectroscopy

FT-IR analyses in the 4000–550 cm^{-1} region were conducted using an FT-IR System 2000 (PerkinElmer, Waltham, MA, USA) with KBr as the medium.

2.4.2. Thermogravimetric Analysis

TGA analysis was performed with a TGA TA instrument Q500 according to the following method: heating under a nitrogen blanket from 30 °C to 300 °C at 10 °C/min, isothermal step at 300 °C for 15 minutes, heating to 550 °C at 20 °C/min, isothermal step for 15 minutes, heating to 900 °C at 10 °C/min, isothermal step for 3 minutes, shift from nitrogen to air, final isothermal step for 30 minutes.

2.4.3. Scanning electron microscopy coupled with energy-dispersive X-ray spectroscopy

The SEM-EDX investigation was carried out using a Zeiss EVO 50 EP SEM (Zeis Vision Care, Castiglione Olana, Italy) coupled with an EDX spectrometer (Bruker Quantax 200 6/30, Bruker, Billerica USA). Sample powders were applied on aluminum stubs with a conductive carbon biadhesive. The samples were subsequently coated with gold using an Ewards S150B sputter coater (Perkin Elmer Milan, Italy) and evaluated.

2.4.4. High-resolution transmission electron microscopy

HRTEM micrographs on HNT-K6/Cu sample taken from sonicated suspensions of the material in ethyl acetate were carried out with a Philips CM 200 field emission gun microscope operating at an accelerating voltage of 200 kV. A few drops of the suspension were deposited on a 200-mesh lacey carbon-coated copper grid and air-dried for several hours before analysis. During the acquisition of HRTEM images, the samples did not undergo structural transformation. Low beam current densities and short acquisition times were adopted. The Gatan Digital Micrograph software was used to estimate the dimensions of the Cu particles.

3. Results and discussion

3.1. Synthesis

Inspired by our recent work, where the hybrid material HNT-K reported in Fig. 1 was employed as an antibacterial, leveraging the chelating action of K, and simultaneously as a nanocontainer for the delivery of resveratrol and curcumin [28], we modified the synthetic approach to enhance the functionalization degree of the material. This was achieved by increasing the weight percentage of K (from 1:1–1:6 HNT:K wt/wt) and adjusting the molar ratio (from 2 to 10 equivalents) of triethylamine (Et_3N) relative to K (Table 1).

To catalyze the photoconversion of CO_2 into methane, by exploiting K's chelating capabilities that favor the reaction due to the presence of copper ions [37], the HNT-K/Cu^{1+} complex was formed in the presence of $CuCl_2$ and H_2O, followed by a reduction reaction in the presence of ascorbic acid (Fig. 2) [29].

3.2. Characterizations

Initially, we aimed to compare the series of functionalized materials employing FT-IR spectra. Fig. 3 presents the FT-IR spectra of pristine HNTs and the HNT-K series, demonstrating the successful functionalization of HNTs with K. In the spectrum of the HNTs (black line), the bands related to the OH groups are evident: the peak at 908 cm^{-1} is attributable to the Al-O-OH vibration, while the bands at 3694 and 3622 cm^{-1} are due to the stretching vibrations of the Al-OH groups. Furthermore, a strong O-Si-O peak is observed around 1070 cm^{-1}, while the peak at 753 cm^{-1} can be assigned to the apical Si-O stretching mode [5,10,38]. As the amount of K increases (dashed lines), the presence of these peaks decreases, indicating successful functionalization. In addition to the presence of signals related to HNTs, those typical of K are evident: at 2988 and 3073 cm^{-1}, the average of CH_2 stretching vibrations; at 1658 cm^{-1}, a strong signal related to the C═O conjugated ketone; at 1629 cm^{-1}, the C═C stretching typical of an unsaturated ketone; finally, at 1220 cm^{-1}, the C-O stretching associated with K [28]. These changes in the FT-IR spectra confirm the successful functionalization between the HNTs and K throughout the HNT-K series (dotted lines).

Thermogravimetric analysis (TGA) was performed to investigate the new material's thermal stability and degree of functionalization. Table 2 shows the mass loss percentages of the pristine materials (HNT and K), the entire HNT-K series, and the samples in the presence of Cu. Mass losses are characteristic of pure materials. As we move from HNT-K1 to HNT-K6, the decreasing residue at 900 °C reflects increased organic content, confirming enhanced functionalization. The degree of functionalization (%f, Table 2) for all HNT-K samples was calculated using Eq. 7, where x is the mass loss between 150 °C and 550 °C.

$$\%f = \frac{x_{adduct} - x_{hnt}}{x_K - x_{hnt}} \times 100 \quad (7)$$

The observed increase in the %f is consistent with the enhanced catalytic capacity of the material. The higher amount of K loaded on the surface, particularly in HNT-K6, correlates with its improved catalytic

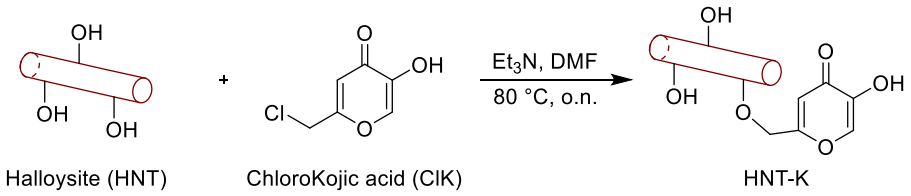

Fig. 1. Reaction scheme for synthesizing HNT-K material.

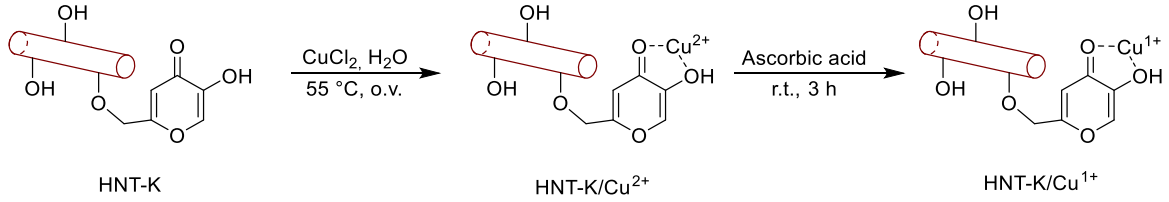

Fig. 2. Reaction scheme for the formation of the HNT-K/Cu^{1+} complex.

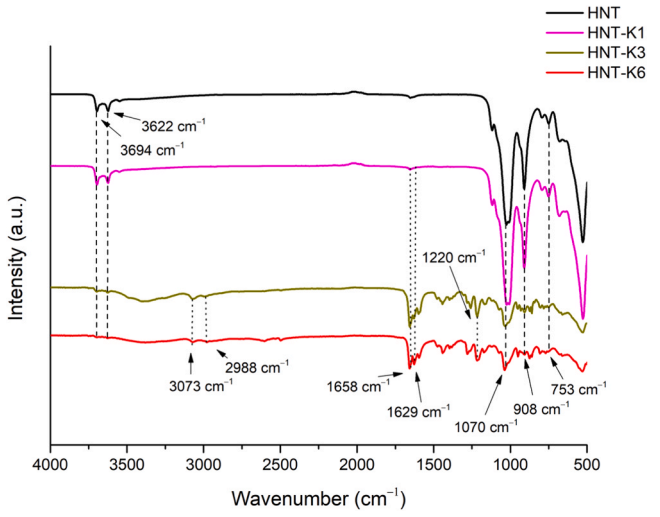

Fig. 3. Stacked FT-IR spectra of pristine HNT(black line), HNT-K1 (pink line), HNT-K3 (green line), and HNT-K6 (red line).

performance.

Considering the improved catalytic activity displayed by the HNT-K6 material, to also explore the potential of green solvents, we investigated the synthesis of HNT-K6 using 2-methyltetrahydrofuran (2-MeTHF) and cyclopentyl methyl ether (CPME) instead of DMF. This aims to assess the impact of these solvents on the degree of functionalization and catalytic performance. Unfortunately, among the solvents tested, DMF provided the highest %*f* for HNT-K6, resulting in a residue of 18 %, indicating the most effective functionalization.

To evaluate the thermal stability of the samples containing Cu, TGA was conducted both before (B) and after (A) their use as catalysts in the photocatalytic CO_2 reduction reaction.

It is essential to underline that copper-based samples exhibit significantly higher inorganic residue. Notably, HNT-K6 contains the highest amount of K, which enhances its ability to chelate cations effectively. Specifically, the residue in HNT-K6/Cu/A increases to 84.4 % from 18 % in HNT-K6. Furthermore, HNT-K6/Cu shows similar residue levels before (B) and after (A) the catalytic activity, indicating good stability throughout the catalytic cycle. In contrast, the non-functionalized nanotubes (HNT/Cu) and HNT-K1/Cu display high residue levels that are not significantly different from those without Cu, highlighting their poor capacity to bind copper. HNT-K3/Cu demonstrates a change in residue amount before (B) and after (A) the catalytic activity; such behavior justifies its lower catalytic capacity.

The morphological studies of the surface and elemental analysis of HNT, HNT-K6, and HNT-K6/Cu were performed by SEM coupled with EDX (Fig. 4); EDX graphs are provided in the supplementary material (Figs. S6–S10. Besides SEM images and EDX graphs, the supplementary material also includes micrographs of HNT-K6 synthesized with 2-MeTHF and CPME (Figs. S11 and S12).

In Fig. 4a, globular agglomerates of pristine HNT are observed. These agglomerates become more compact after the functionalization of HNT with K, as shown in Fig. 4b. However, the surface of the HNT-K6

Table 2
The mass loss percentages of pristine HNT and K, the entire HNT-K series, and the HNT-K series with Cu(I) before (B) and after (A) catalysis.

Mass Loss %							
Sample	**T < 150 °C**	**150 °C < T < 350 °C**	**350 °C < T < 550 °C**	**550 °C < T< 900 °C**	**Residue**	**Amount of Cu**	**%*f***
HNT	2.3	1.3	12.2	0.3	83.9	—	—
K	1.8	98.2	—	—	-	—	—
HNT-K1	0.3	1.9	12.8	0.8	84.2	—	1.4
HNT-K3	2.0	35.6	16.0	21.1	25.3	—	45.0
HNT-K6 2-MeTHF	0.8	5.0	15.3	2.2	76.7	—	8.0
HNT-K6 DMF	1.7	43.7	16.3	20.2	18.1	—	54.9
HNT-K6 CPME	1.8	13.7	20.8	8.5	55.2	—	24.8
HNT/Cu	0.7	1.7	8.9	1.3	87.4	3.5	—
HNT-K1/Cu/B	0.6	2.2	8.4	1.3	87.5	3.3	1.4
HNT-K1/Cu/A	0.5	2.6	8.8	1.5	86.6	2.4	1.4
HNT-K3/Cu/B	0.6	4.7	19.3	8.9	66.5	41.2	45.0
HNT-K3/Cu/A	0.5	3.0	12.6	4.1	79.8	54.3	45.0
HNT-K6/Cu/B	0.4	5.4	10.2	0.6	83.4	28.2	54.9
HNT-K6/Cu/A	0.6	4.0	10.8	0.2	84.4	29.2	54.9

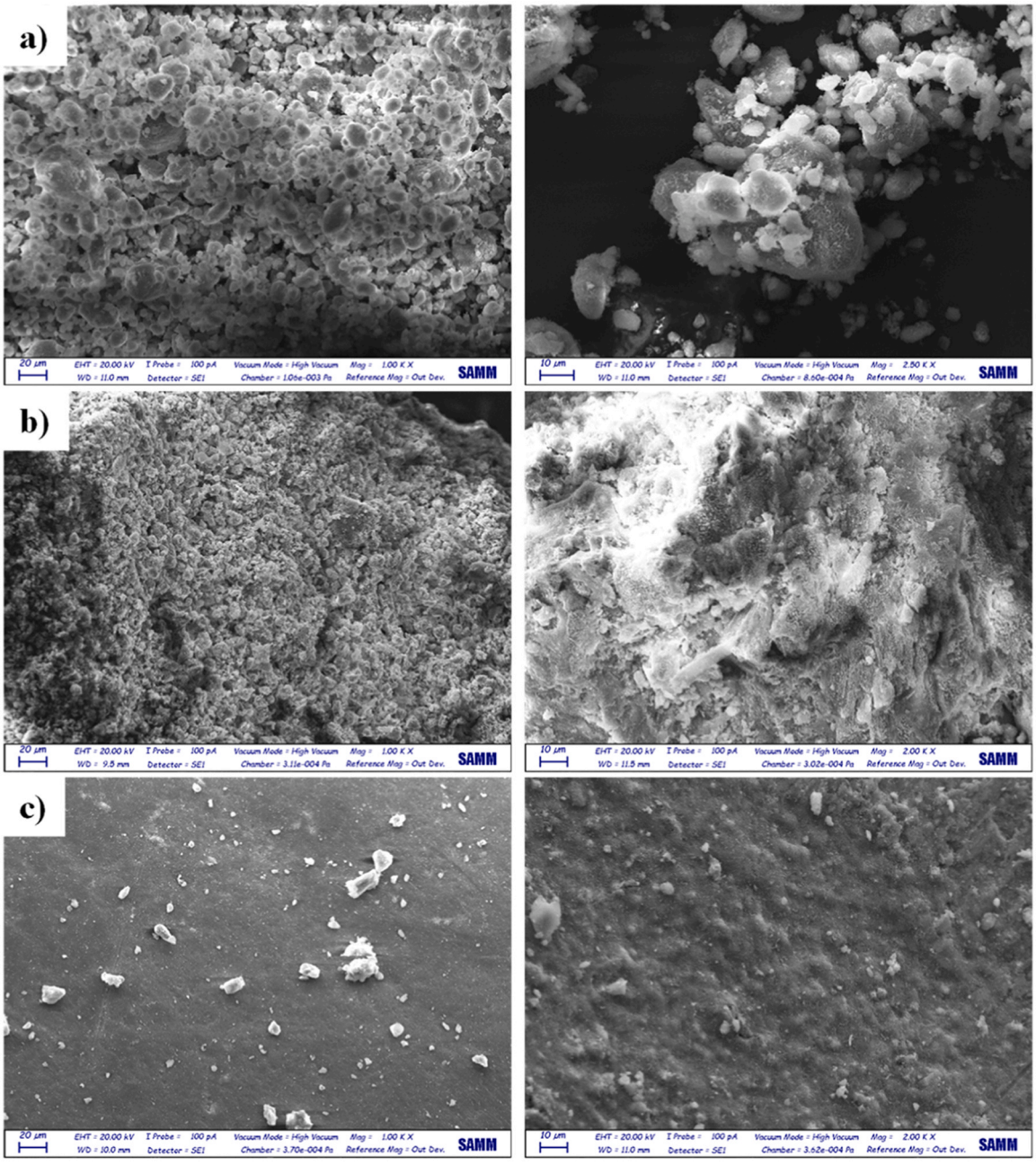

Fig. 4. SEM images of pristine HNT (a), HNT-K6 in DMF (b), and HNT-K6/Cu (c).

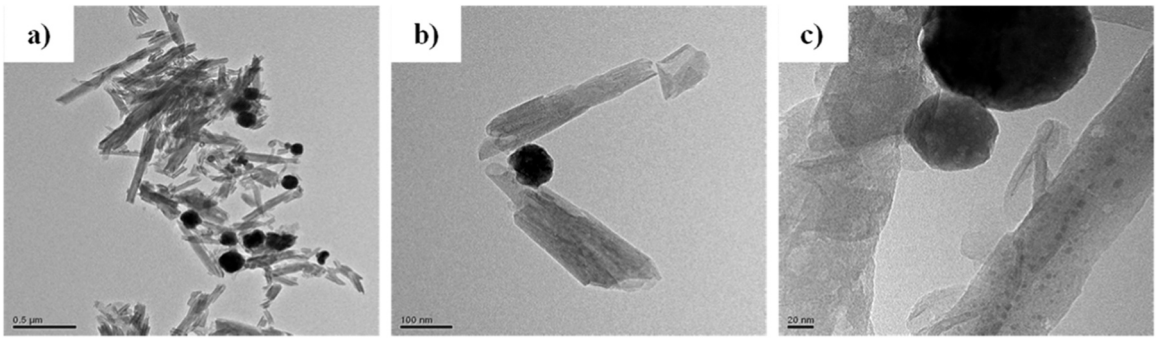

Fig. 5. Micrographs of HNT-K6/Cu. Bright-field TEM micrograph at low magnification (a). HR-TEM micrographs (b and c).

material appears coarser. Conversely, the presence of Cu deposited on the surface of the HNT/K6 smoothens the surface, with only a few agglomerates remaining visible. The EDX analysis, as reported in the supplementary material, revealed the presence of Cl in the HNT-K6 (Fig. S7) and HNT-K6/Cu (Fig. S10) samples compared to the pristine HNT, confirming the presence of Cu in the HNT-K6/Cu samples.

A thorough morphological investigation of the HNT-K6/Cu sample was conducted using TEM and HR-TEM (Fig. 5). This analysis aimed to determine whether the morphology was maintained after functionalization and copper decoration. Deposition of an adequate amount of sample enabled statistical analysis of the material morphology and metal dispersion. An ethyl acetate suspension of HNT-K6/Cu, with a 1 mg/mL concentration, was sonicated for 5 minutes using an ultrasonic bath. Subsequently, the suspension was analyzed, and micrographs were captured at lower and higher magnification (Fig. 5). The micrographs taken at high magnification in Fig. 5 reveal a regular nanotube skeleton. Such observations facilitated the detection of the mean dimensions of the copper particles, ranging from 60 to 140 nm.

3.3. Catalytic activity

All synthesized composites (HNT-K1,3,6) were initially tested for their catalytic capabilities for CO_2 photoconversion in the presence of Cu (I). HNT-K6 was also studied in the presence of Cu(II) (Table 3). The reaction was conducted over 7 h of simulated solar irradiation with H_2 as the reducing agent (see the details in the experimental section). Under these conditions the H_2 molecules dissociate into hydrogen atoms on the surface of the metal, which can then hydrogenate the adsorbed CO_2 [30, 33].

In our experimental conditions, only CO and CH_4 were detected as the main products of the reaction. Consistent with literature findings, the presence of the Cu ions favored the selectivity towards methane [26, 37,39]; specifically, the presence of the cuprous ions was essential to enhance the CH_4 formation [25,40–42]. Therefore, comparing the performance of the HNT-K6/Cu(II) with the corresponding HNT-K6/Cu(I) samples, it is evident that the latter material significantly increased the CO_2 conversion by approximately threefold, resulting in a fourfold increase of the CH_4 selectivity (Table 3, Entry 8 *vs*. Entry 7). This aligns with the literature data, with the cuprous species that better promote CO_2 reduction than the corresponding cupric ions [25,40,43]. Specifically, under the simulated solar irradiation, the H_2 molecules were dissociated into H^+, and they were able to react with the adsorbed CO_2 on the basic sites of the halloysite. The presence of the chelated Cu (I) ions catalyzed the afterward reduction of CO_2 into CO and successively into methane [44]. The increase in K content benefitted the photocatalytic activity, likely due to its enhanced capability to chelate the Cu (I) ions, which are the active reaction species. The optimum performance was achieved with the HNT-K6/Cu(I) sample (Table 3, Entry 7). However, further increases in K content were detrimental (results not shown), possibly because an excess of acid hindered photon absorption on the Cu(I) sites. The catalyst without the K functionalization, HNT/Cu (I) (Table 3, Entry 4), exhibited low photoactivity, confirming that the chelating action of K is crucial for enabling an efficient activation of the photocatalytic reaction on the cuprous ions sites. As expected, the bare HNT, K, and HNT-K compounds (Table 3, Entries 1–3) did not photoconvert CO_2 due to the absence of photocatalytically active sites that promote CO_2 reduction. While comparing results across literature studies can be challenging due to variations in experimental setups and conditions (such as the type of lamp used, duration of irradiation, temperature, etc.), the results obtained with the HNT-K6/Cu(I) sample are noteworthy in terms of CH_4 selectivity and yield, considering that in the same experimental conditions, the typical Cu_2O/TiO_2-based semiconductor oxides, although showed a higher CO_2 conversion (45 %), primarily promoted the CO formation, with a selectivity of 67 %, rather than the CH_4 formation, which had a selectivity of only 33 % [25]. *Deng. et al.* obtained a remarkable CH_4 selectivity of 97 % using a Cu^0 decorated on Cu_2O [41]. Considering that in the case at hand the copper ions are present only as chelated ions within the hybrid composite structure rather than being directly decorated on a metal oxide surface, the results are promising and align well with the literature data.

Furthermore, Fig. 6 reports the photocatalytic stability of the best-performing sample, HNT-K6/Cu(I), after four consecutive runs of the photocatalytic reaction. The sample exhibited good stability, with only a slight decrease in the CO_2 conversion after the fourth run (equivalent to 28 h of simulated solar irradiation). This minor reduction in performance can be reasonably attributed to the partial oxidation of Cu(I) into Cu(II), which, as discussed previously, are less photoactive compared to the cuprous ions. Despite this, the overall stability of the HNT-K6/Cu(I) catalyst remains satisfactory, indicating its potential for practical application in CO_2 photoconversion processes.

HNT-K has also been employed as a sustainable catalyst for the fixation of CO_2 into cyclic carbonates through its reaction with epoxides. Styrene epoxide (**1a**) was used as the model substrate to produce carbonate **1b** (Fig. 7). The initial strategy aimed to exploit the chelating abilities of the kojic acid bound to HNT to coordinate with copper, hypothesizing that this could catalyze the CO_2 fixation reaction. In this study, we first screened all synthesized materials with different ratios of

Table 3
Screening of catalysts used for the photocatalytic CO_2 reduction.[a].

Entry	Sample	CO_2 conversion after 7 hours of solar radiation (simulated)	CH_4 selectivity	CO selectivity	CH_4 yield
1	HNT	—	/	/	/
2	K	—	/	/	/
3	HNT-K	—	/	/	/
4	HNT/Cu (I)	7.6 %	57.1 %	41.9 %	4.3 %
5	HNT-K1/Cu (I)	9.2 %	59.6 %	39.4 %	5.5 %
6	HNT-K3/Cu (I)	14.3 %	65.4 %	33.6 %	9.4 %
7	HNT-K6/Cu (I)	31.3 %	78.5 %	20.5 %	24.5 %
8	HNT-K6/Cu (II)	10.4 %	19.6 %	79.4 %	2.0 %

[a] Reaction conditions: catalyst (100 mg), CO_2 and H_2 1 atm, H_2:CO_2 molar ratio (4:1), 7 h of solar radiation (simulated), T = 45 °C, due to the heating of the solar lamp.

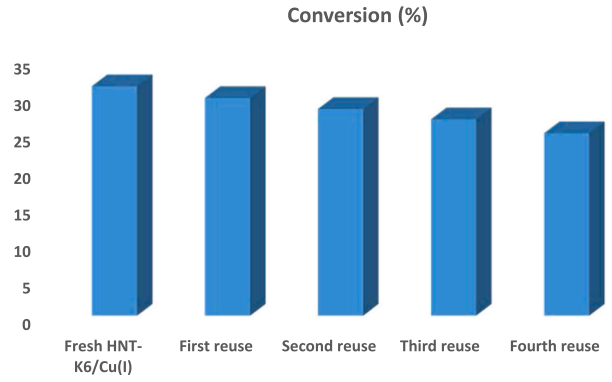

Fig. 6. Photocatalytic consecutive runs (each run of 7 h of simulated solar irradiation) for the HNT-K6/Cu(I) sample in the CO_2 reduction reaction. After each run, before performing the following one, the photocatalyst was treated in He flows (30 mL/min) for 2 h to remove eventual contaminants from the sample surface.

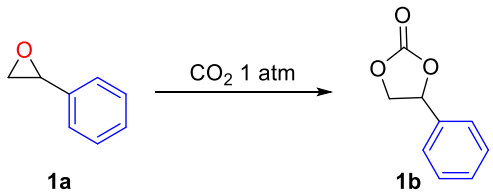

Fig. 7. Model reaction between styrene epoxide and CO_2.

HNT to K, as well as individual non-functionalized substrates (Table 4). The best result was achieved with the HNT-K6 and TBAB without Cu (Table 4, Entry 10). Surprisingly, the test performed in Cu(II) presence resulted in lower yields than those without copper (Table 4, Entry 12).

The ability of HNT-K6 to catalyze the reaction in the absence of metals allows us to infer that the presence of K plays a crucial role in retaining CO_2 and opening the epoxide ring. This catalysis occurs without solvents at relatively low temperatures, especially at atmospheric pressure. Once the catalytic ability of HNT-K6 was verified, we proceeded to vary the catalyst ratios to styrene oxide to optimize the reaction conditions (Table 5).

The optimum conditions were reached with a ratio of **1a**:HNT-K6 of 20:1 (Table 5, Entry 4). Again, there is a synergistic effect between HNT and K, as demonstrated in the photoconversion of CO_2 to CH_4 and the fixation of CO_2 into cyclic carbonates; HNT-K6 proved to be the superior catalyst for these processes, as we expected considering the higher *%f* (54.9, Table 2). Subsequently, the reaction was extended to other substrates (**2a**–**5a**, Table 6), achieving good yields at 1 atm CO_2 in the absence of Cu. While Cu ions were required to create active sites in the photocatalytic CO_2 reduction process, the fixation of CO_2 into cyclic carbonates benefited from the synergy between HNT and K without the necessity for Cu ions.

Through CO_2 adsorption studies (see the CO_2 breakthrough curves reported in Fig. S13), we observed that the presence or absence of copper on the surface of HNT-K6 significantly impacts its adsorption capacity. Specifically, the HNT-K6 exhibited a higher ability to retain the CO_2, reaching saturation at a higher time (85 min), indicating greater CO_2 capture than the HNT-K6/Cu(II), which reached saturation in about 22 min. This finding suggests that HNT-K6, without copper, is more effective at catalyzing the CO_2 fixation into carbonates. This is because K, when not chelating copper, can freely interact with CO_2 and epoxides. Based on the proposed mechanisms of CO_2 conversion [45] and the experimental evidence that K must be free to interact with CO_2, the proposed mechanism for our conversion relies on the H-bond activation instead of the transition metal activation (Fig. 8). To further support this observation, we conducted a hydrogen-deuterium exchange of the HNT-K6 catalyst. The obtained deuterated catalyst, namely HNT-K6D, was then used for the CO_2 fixation reaction under the same conditions as in Table 6, entry 1, with a conversion of only 22 % in accordance with the deuterium effect [46].

Table 4
Screening of catalysts and co-catalyst.[a].

Entry	Catalyst	Co-Catalyst	Conversion[b] (%)
1	HNT	—	—
2	HNT	TBAB	—
3	K	—	—
4	K	TBAB	35
5	—	TBAB	20
6	HNT-K1	TBAB	6
7	HNT-K1	—	—
8	HNT-K3	TBAB	67
9	HNT-K3	—	10
10	HNT-K6	TBAB	87
11	HNT-K6	—	18
12	HNT-K6/Cu(II)	TBAB	23

[a] Reaction conditions: **1a** (10 mmol), Catalyst (5 %wt), TBAB co-catalyst (0.5 mmol), 70 °C, 10 h CO_2 1 atm.
[b] Conversion was calculated by ^{1}H NMR. Selectivity > 99 %.

Table 5
Effect of different **1a**:HNT-K6 ratios on the conversion of styrene oxide.[a].

Entry	1a:HNT-K6 (wt:wt)	Conversion[b] (%)
1	1:1	89
2	5:1	87
3	10:1	87
4	20:1	87
5	30:1	55
6	40:1	33

[a] Reaction conditions: **1a** (10 mmol), TBAB (0.5 mmol), 70 °C, 10 h, CO_2 1 atm.
[b] Conversion was calculated by ^{1}H NMR. Selectivity > 99 %.

Reusability experiments were carried out by periodically injecting the same quantity of TBAB (Fig. 9) into the reaction mixture after the isolation of the products. Specifically, the reaction crude was mixed with 1 mL of chloroform, and the resulting mixture was centrifuged to extract the remaining HNT-K6, which is not soluble in the organic solvent. The HNT-K6 was vacuum-dried for reuse in subsequent processes after TBAB was added. The reusability experiments showed that HNT-K6 demonstrated outstanding catalytic capacity, with a conversion rate exceeding 90 % in the first two reuses. In the third and fourth reuses, the conversion rates fell to 85 % and 70 %, respectively. These results indicate that HNT-K6 retains good catalytic efficacy over multiple cycles, illustrating the material's durability and effectiveness. The slight decline in conversion efficiency after the third reuse suggests that while HNT-K6 remains effective, some gradual deactivation occurs. Nevertheless, the material continues to function effectively even after the third usage, indicating its suitability as a catalyst for recurring reactions.

To highlight the excellent catalytic ability of HNT-K6 in CO_2 fixation, we compared it with other clay and aluminosilicate catalysts for the conversion of styrene oxide (Table 7). From the comparison, it is easy to see that HNT-K6 is an excellent compromise regarding reaction conditions (temperature, CO_2 pressure and time), the absence of metals, and the simple synthetic procedure for obtaining it.

4. Conclusion

In summary, this study presents a straightforward synthesis approach for creating a hybrid material consisting of HNT and K, serving as an efficient catalyst for CO_2 conversion processes. Copper ions are smoothly deposited onto the material surface by utilizing the chelating properties of K, providing a cost-effective alternative to noble metals for catalyzing reactions. This hybrid catalyst demonstrates remarkable efficacy in facilitating two distinct CO_2 conversion pathways, which are the photoconversion of CO_2 in methane under simulated sunlight exposure and the fixation of CO_2 into cyclic carbonates. With 31 % and 89 % conversion achieved for photocatalytic CO_2 reduction and carbonate fixation, respectively, the hybrid and bio-based material notably demonstrates good catalytic activity under mild reaction conditions, maintaining high conversion efficiencies at atmospheric pressure and moderate temperatures (45 °C for methane conversion and 70 °C for carbonate fixation). Additionally, its organic/inorganic hybrid nature is complemented by excellent thermal stability, enabling repeated utilization. Overall, this research underscores the promising potential of harnessing naturally derived materials such as the one here reported for sustainable CO_2 utilization, offering a valuable contribution to green chemistry and environmental sustainability, underscoring the practical utility compared to many catalysts reported in the literature.

CRediT authorship contribution statement

Vincenzina Barbera: Writing – review & editing, Supervision, Resources, Formal analysis, Funding acquisition. **Roberto Fiorenza:**

Table 6
Reaction on different substrates.[a].

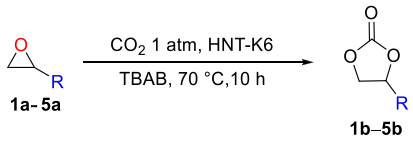

Entry	Reagent	Product	Yield (%)	Yield (%)[b]	TOF[c]
1	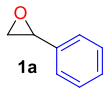	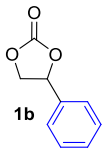	85	16	2.62
2		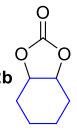	44	8	1.6
3	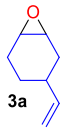	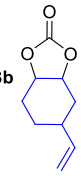	35	5	1.1
4	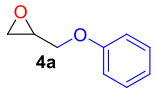	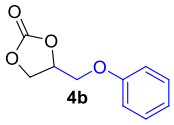	20	3	0.82
5		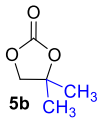	71	11	3.94

[a] Reaction conditions: epoxide (10 mmol), HNT-K6 (5 % wt), TBAB (0.5 mmol), 70 °C, 10 h CO_2 1 atm.
[b] Yield obtained in the presence of TBAB alone (0.5 mmol). [c] TOF (h^{-1}), see Eq. 6.

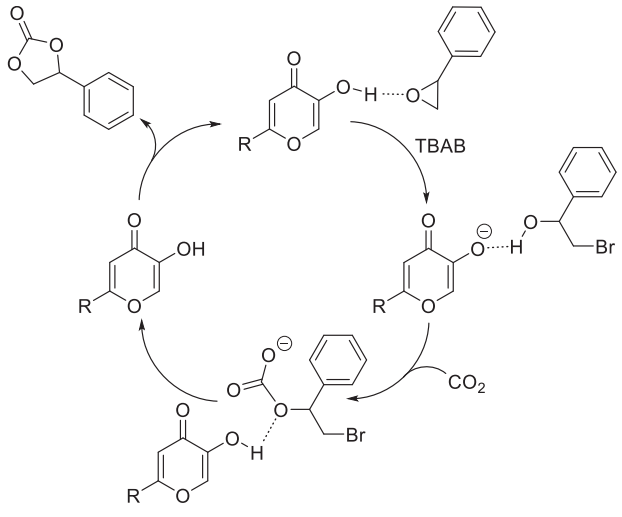

Fig. 8. Proposed mechanism for the conversion.

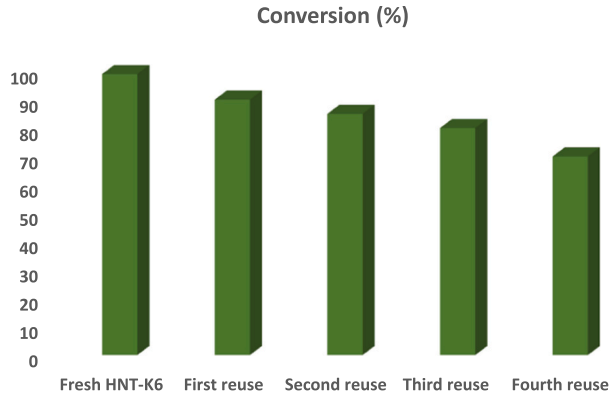

Fig. 9. Catalyst reusability study for the model reaction with HTN-K6; the conditions used are the same as reported in Table 5 Entry 4.

Visualization, Validation, Supervision, Resources, Methodology, Investigation. **Monia Camarda:** Methodology, Investigation. **Giusy Dativo:** Methodology, Investigation. **Federica Magaletti:** Writing – original draft, Methodology, Investigation. **Vincenzo Patamia:** Writing – review & editing, Writing – original draft, Visualization, Supervision, Project administration, Formal analysis, Conceptualization. **Erika Saccullo:** Visualization, Validation, Methodology, Investigation. **Antonio Rescifina:** Writing – review & editing, Resources, Project administration, Funding acquisition. **Giuseppe Floresta:** Supervision, Resources, Project administration, Conceptualization.

Table 7
Comparison of catalytic activity with clay-based catalysts on the conversion of styrene oxide.

Catalyst	Temperature, pressure and time	Co-Catalyst	Metal	Conversion (%)	Reference
IL@P-BC	100 °C, 3 MPa, 12 h	TBAB	No	90	[47]
MIL-101 (Cr)/ AC-2	40 °C, 1 atm, 48 h	TBAB	Yes	99	[48]
1-Mont	100 °C, 1 atm, 24 h	TBAB	Yes	99	[49]
Talc	140 °C, 30 bars, 12 h	TBAB	No	91	[50]
ZIF-8/ ATP	120 °C, 1 MPa, 1 h	TBAB	Yes	92	[51]
HNT-K6	70 °C, 1 atm, 10 h	TBAB	No	89	This work

Declaration of Competing Interest

The authors declare that they have no known competing financial interests or personal relationships that could have appeared to influence the work reported in this paper.

Data availability

Data will be made available on request.

Acknowledgements

The research leading to these results has received funding from the European Union—NextGen-erationEU through the Italian Ministry of University and Research under PNRR—M4C2-I1.3 Project PE_00000019 “HEAL ITALIA” (Antonio Rescifina, Vincenzo Patamia and Erika Saccullo), CUP E63C22002080006. Roberto Fiorenza thanks the Starting Grant PIACERI 2020–2022 of the University of Catania for the support. Giusy Dativo thanks the Sicilian Micro and Nano Technology Research and Innovation Center (SAMOTHRACE, CUP E63C22000900006) for funding the Ph.D. grant. The views and opinions expressed are those of the authors only and do not necessarily reflect those of the European Union or the European Commission. Neither the European Union nor the European Commission can be held responsible for them. Pirelli Tyre is gratefully acknowledged for financing the PhD activity of Federica Magaletti.

Appendix A. Supporting information

Supplementary data associated with this article can be found in the online version at doi:10.1016/j.jcou.2024.102865.

References

[1] A. Abotaleb, D. Al-Masri, A. Alkhateb, K. Mroue, A. Zekri, Y. Mashhour, A. Sinopoli, Assessing the effect of acid and alkali treatment on a halloysite-based catalyst for dry reforming of methane, RSC Adv. 14 (7) (2024) 4788–4803.
[2] K. Peng, J. Ye, H. Wang, H. Song, B. Deng, S. Song, Y. Wang, L. Zuo, J. Ye, Natural halloysite nanotubes supported Ru as highly active catalyst for photothermal catalytic CO2 reduction, Appl. Catal. B: Environ. 324 (2023) 122262.
[3] X. Li, Y. Jiang, R. Zhou, Z. Hou, Acetalization of glycerol with acetone over appropriately-hydrophobic zirconium organophosphonates, Appl. Clay Sci. 189 (2020) 105555.
[4] K. Ramadass, C. Sathish, S. MariaRuban, G. Kothandam, S. Joseph, G. Singh, S. Kim, W. Cha, A. Karakoti, T. Belperio, Carbon nanoflakes and nanotubes from halloysite nanoclays and their superior performance in CO2 capture and energy storage, ACS Appl. Mater. Interfaces 12 (10) (2020) 11922–11933.
[5] V. Patamia, R. Fiorenza, C. Zagni, S. Agustin-Salazar, S. Scirè, G. Floresta, A. Rescifina, TiO2/Loofah–halloysite bio–hybrid composites as efficient systems for VOCs removal, Chem. –A Eur. J. (2024) e202304276.
[6] A. Pechenkin, D. Potemkin, S. Badmaev, E. Smirnova, K. Cherednichenko, V. Vinokurov, A. Glotov, CO2 hydrogenation to dimethyl ether over In2O3 catalysts supported on aluminosilicate halloysite nanotubes, Green. Process. Synth. 10 (1) (2021) 594–605.
[7] M. Massaro, R. Noto, S. Riela, Past, present and future perspectives on halloysite clay minerals, Molecules 25 (20) (2020) 4863.
[8] J. Wang, Y. Zhang, J. Si, W. Zhang, Q. Liang, W. Li, B. Jin, S. Miao, Structural engineering of NiFe-Layered double hydroxides and halloysite composites for efficient CO2 capture, Chem. Eng. J. 463 (2023) 142502.
[9] A. Pechenkin, D. Potemkin, M. Rubtsova, P. Snytnikov, P. Plyusnin, A. Glotov, CuO-In2O3 catalysts supported on halloysite nanotubes for CO2 hydrogenation to dimethyl ether, Catalysts 11 (10) (2021) 1151.
[10] V. Patamia, R. Fiorenza, I. Brullo, M.Z. Marsala, S.A. Balsamo, A. Distefano, P. M. Furneri, V. Barbera, S. Scirè, A. Rescifina, A sustainable porous composite material based on loofah-halloysite for gas adsorption and drug delivery, Mater. Chem. Front. 6 (16) (2022) 2233–2243.
[11] Z. Wang, Y. Pang, H. Guo, H. Wang, L. Liu, X. Wang, S. Zhang, W. Cui, Increased CO2 capture capacity via amino-bifunctionalized halloysite nanotubes adsorbents, Fuel 364 (2024) 131036.
[12] W. Ma, Y. Zhu, X. Wang, Au nanoparticles modified HNTs/g-C3N4/CdS composite for highly efficient CO2 photoreduction and tetracycline degradation, J. Alloy. Compd. 935 (2023) 168129.
[13] W.K. Fan, M. Tahir, Structured clay minerals-based nanomaterials for sustainable photo/thermal carbon dioxide conversion to cleaner fuels: a critical review, Sci. Total Environ. 845 (2022) 157206.
[14] K. Fernández-Caso, G. Díaz-Sainz, M. Alvarez-Guerra, A. Irabien, Electroreduction of CO2: advances in the continuous production of formic acid and formate, ACS Energy Lett. 8 (4) (2023) 1992–2024.
[15] J.A. Abarca, G. Díaz-Sainz, I. Merino-Garcia, A. Irabien, J. Albo, Photoelectrochemical CO2 electrolyzers: from photoelectrode fabrication to reactor configuration, J. Energy Chem. (2023).
[16] A. Kilic, E. Aytar, C. Okcu, M. Durgun, An improved boron-catalyzed cycloaddition of CO2 to epoxides for the production of five-membered cyclic carbonates under atmospheric versus high-pressure conditions, Sustain. Chem. Pharm. 39 (2024) 101620.
[17] A. Kilic, A. Alhafez, E. Aytar, R. Soylemez, The sustainable catalytic conversion of CO2 into value-added chemicals by using cobaloxime-based double complex salts as efficient and solvent-free catalysts, Inorg. Chim. Acta 554 (2023) 121547.
[18] A. Alhafez, E. Aytar, A. Kilic, Enhancing catalytic strategy for cyclic carbonates synthesized from CO2 and epoxides by using cobaloxime-based double complex salts as catalysts, J. CO2 Util. 63 (2022) 102129.
[19] A. Kilic, B. Sobay, E. Aytar, R. Söylemez, Synthesis and effective catalytic performance in cycloaddition reactions with CO 2 of boronate esters versus N-heterocyclic carbene (NHC)-stabilized boronate esters, Sustain. Energy Fuels 4 (11) (2020) 5682–5696.
[20] M. Ulusoy, O. Şahin, A. Kilic, O. Büyükgüngör, Multinuclear Cu (II) Schiff base complex as efficient catalyst for the chemical coupling of CO 2 and epoxides: synthesis, X-ray structural characterization and catalytic activity, Catal. Lett. 141 (2011) 717–725.
[21] R. Bentley, From miso, sake and shoyu to cosmetics: a century of science for kojic acid, Nat. Prod. Rep. 23 (6) (2006) 1046–1062.
[22] V.M. Nurchi, J.I. Lachowicz, G. Crisponi, S. Murgia, M. Arca, A. Pintus, P. Gans, J. Niclos-Gutierrez, A. Domínguez-Martín, A. Castineiras, Kojic acid derivatives as powerful chelators for iron (III) and aluminium (III), Dalton Trans. 40 (22) (2011) 5984–5998.
[23] C. Zagni, V. Patamia, S. Dattilo, V. Fuochi, S. Furnari, P.M. Furneri, S.C. Carroccio, G. Floresta, A. Rescifina, Supramolecular biomaterials as drug nanocontainers with iron depletion properties for antimicrobial applications, Mater. Adv. 5 (9) (2024) 3675–3682.
[24] B. Singh, K. Suri, K. Shevkani, A. Kaur, A. Kaur, N. Singh, Enzymatic browning of fruit and vegetables: a review, Enzym. Food Technol.: Improv. Innov. (2018) 63–78.
[25] R. Fiorenza, C. Contarino, V. Spanò, M.T.A. Iapichino, S.A. Balsamo, Photothermo-catalytic strategies for the CO2 valorisation using TiO2-based composites, Catal. Today 423 (2023) 114251.
[26] R. Fiorenza, M. Bellardita, S.A. Balsamo, L. Spitaleri, A. Gulino, M. Condorelli, L. D'Urso, S. Scirè, L. Palmisano, A solar photothermocatalytic approach for the CO2 conversion: Investigation of different synergisms on CoO-CuO/brookite TiO2-CeO2 catalysts, Chem. Eng. J. 428 (2022) 131249.
[27] R. Hariri, S. Dehghanpour, Effective visible-light CO2 photoreduction over (metallo) porphyrin-based metal–organic frameworks to achieve useful hydrocarbons, Appl. Organomet. Chem. 35 (12) (2021) e6422.
[28] V. Patamia, C. Zagni, R. Fiorenza, V. Fuochi, S. Dattilo, P.M. Riccobene, P. M. Furneri, G. Floresta, A. Rescifina, Total bio-based material for drug delivery and iron chelation to fight cancer through antimicrobial activity, Nanomaterials 13 (14) (2023) 2036.
[29] J. Xiong, Y. Wang, Q. Xue, X. Wu, Synthesis of highly stable dispersions of nanosized copper particles using L-ascorbic acid, Green. Chem. 13 (4) (2011) 900–904.
[30] Y. Chen, Y. Zhang, G. Fan, L. Song, G. Jia, H. Huang, S. Ouyang, J. Ye, Z. Li, Z. Zou, Cooperative catalysis coupling photo-/photothermal effect to drive Sabatier reaction with unprecedented conversion and selectivity, Joule 5 (12) (2021) 3235–3251.
[31] S. Kumar, M. Regue, M.A. Isaacs, E. Freeman, S. Eslava, All-inorganic CsPbBr3 nanocrystals: gram-scale mechanochemical synthesis and selective photocatalytic CO2 reduction to methane, ACS Appl. Energy Mater. 3 (5) (2020) 4509–4522.

[32] B. Rhimi, M. Zhou, Z. Yan, X. Cai, Z. Jiang, Cu-based materials for enhanced C2+ product selectivity in photo-/electro-catalytic CO2 reduction: challenges and prospects, Nano-Micro Lett. 16 (1) (2024) 64.
[33] P. Zhang, X. Sui, Y. Wang, Z. Wang, J. Zhao, N. Wen, H. Chen, H. Huang, Z. Zhang, R. Yuan, Surface Ru–H bipyridine complexes-grafted TiO2 nanohybrids for efficient photocatalytic CO2 methanation, J. Am. Chem. Soc. 145 (10) (2023) 5769–5777.
[34] G. Dativo, E. La Greca, L.F. Liotta, V. La Parola, M. Condorelli, G. Impellizzeri, G. Compagnini, S. Sciré, R. Fiorenza, Solar photothermo-catalytic conversion of CO2 on phyllosilicates modified with Ni and CeO2, J. CO2 Util. 82 (2024) 102765.
[35] V. Patamia, D. Gentile, R. Fiorenza, V. Muccilli, P.G. Mineo, S. Scirè, A. Rescifina, Nanosponges based on self-assembled starfish-shaped cucurbit [6] urils functionalized with imidazolium arms, Chem. Commun. 57 (30) (2021) 3664–3667.
[36] V. Campisciano, C. Calabrese, F. Giacalone, C. Aprile, P.L. Meo, M. Gruttadauria, Reconsidering TOF calculation in the transformation of epoxides and CO2 into cyclic carbonates, J. CO2 Util. 38 (2020) 132–140.
[37] R. Long, Y. Li, Y. Liu, S. Chen, X. Zheng, C. Gao, C. He, N. Chen, Z. Qi, L. Song, Isolation of Cu atoms in Pd lattice: forming highly selective sites for photocatalytic conversion of CO2 to CH4, J. Am. Chem. Soc. 139 (12) (2017) 4486–4492.
[38] C. Zagni, A.A. Scamporrino, P.M. Riccobene, G. Floresta, V. Patamia, A. Rescifina, S.C. Carroccio, Portable nanocomposite system for wound healing in space, Nanomaterials 13 (4) (2023) 741.
[39] Q. Chen, Y. Chen, M. Yu, B. Xu, H. Wu, L. Li, J. Bi, Modulating interfacial charges in CTF-based metal-insulator-semiconductor promotes selective CO2 reduction to CH4, Chem. Eng. J. 482 (2024) 149027.
[40] R. Fiorenza, M. Bellardita, S.A. Balsamo, A. Gulino, M. Condorelli, G. Compagnini, S. Scirè, L. Palmisano, A solar photothermo-catalytic combined process for the VOCs combustion and the subsequent CO2 valorization using noble metal-free catalysts, Catal. Today 413 (2023) 113949.
[41] Y. Deng, C. Wan, C. Li, Y. Wang, X. Mu, W. Liu, Y. Huang, P.K. Wong, L. Ye, Synergy effect between facet and zero-valent copper for selectivity photocatalytic methane formation from CO2, ACS Catal. 12 (8) (2022) 4526–4533.
[42] B.-h Li, K.-h Zhang, X.-j Wang, Y.-p Li, X. Liu, B.-H. Han, F.-t Li, Construction synergetic adsorption and activation surface via confined Cu/Cu2O and Ag nanoparticles on TiO2 for effective conversion of CO2 to CH4, J. Colloid Interface Sci. 660 (2024) 961–973.
[43] C.A. Celaya, C. Delesma, S. Torres-Arellano, P. Sebastian, J. Muniz, Understanding CO2 conversion into hydrocarbons via a photoreductive process supported on the Cu2O (1 0 0),(1 1 0) and (1 1 1) surface facets: a first principles study, Fuel 306 (2021) 121643.
[44] E. Baraj, S. Vagaský, T. Hlinčík, K. Ciahotný, V. Tekáč, Reaction mechanisms of carbon dioxide methanation, Chem. Pap. 70 (4) (2016) 395–403.
[45] T. Yan, H. Liu, Z. Zeng, W. Pan, Recent progress of catalysts for synthesis of cyclic carbonates from CO2 and epoxides, J. CO2 Util. 68 (2023) 102355.
[46] R.P. Hanzlik, R.B. Westkaemper, Secondary deuterium isotope effects on epoxide methanolysis reactions, J. Am. Chem. Soc. 102 (7) (1980) 2464–2467.
[47] J. Peng, R. Guo, X. Shi, P. Zhang, F. Qiu, W. Li, C. Wei, S. Miao, Highly efficient and recyclable conversion of CO2 using supported metal-free ionic liquids on ball clay, Appl. Clay Sci. 228 (2022) 106645.
[48] S. Kumari, S. Chakraborty, P. Kanoo, V. Kumar, A. Chakraborty, MIL-101 (Cr)/aminoclay nanocomposites for conversion of CO 2 into cyclic carbonates, Dalton Trans. (2024).
[49] S. Verma, R.I. Kureshy, T. Roy, M. Kumar, A. Das, H.K. Noor-ul, S.H. Abdi, H. C. Bajaj, Immobilization of cationic Al (III) salen in the interlayers of montmorillonite clay for the synthesis of cyclic carbonate, Catal. Commun. 61 (2015) 78–82.
[50] F. Nakibuule, S.A. Nyanzi, I. Oshchapovsky, O.F. Wendt, E. Tebandeke, Synthesis of cyclic carbonates from epoxides and carbon dioxide catalyzed by talc and other phyllosilicates, BMC Chem. 14 (1) (2020) 14.
[51] G. Wang, R. Guo, W. Wang, W. Liu, Natural porous nanorods used for high-efficient capture and chemical conversion of CO2, J. CO2 Util. 42 (2020) 101303.